Slope-assisted BOTDA based on vector SBS and frequency-agile technique for wide-strain-range dynamic measurements

DENGWANG ZHOU,[1] YONGKANG DONG,[1,*] BENZHANG WANG,[1] TAOFEI JIANG,[1] DEXIN BA,[1] PENGBAI XU,[1] HONGYING ZHANG,[2] ZHIWEI LU,[1,4] AND HUI LI[3]

[1]*National Key Laboratory of Science and Technology on Tunable Laser, Harbin Institute of Technology, Harbin 150001, China*
[2]*Institute of Photonics and Optical Fiber Technology, Harbin University of Science and Technology, Harbin 150080, China*
[3]*School of Civil Engineering, Harbin Institute of Technology, Harbin 150001, China*
[4]*lvzw@hit.edu.cn*
[*]*aldendong@gmail.com*

Abstract: We present a slope-assisted BOTDA system based on the vector stimulated Brillouin scattering (SBS) and frequency-agile technique (FAT) for the wide-strain-range dynamic measurement. A dimensionless coefficient K defined as the ratio of Brillouin phase-shift to gain is employed to demodulate the strain of the fiber, and it is immune to the power fluctuation of pump pulse and has a linear relation of the frequency detuning for the continuous pump and Stokes waves. For a 30ns-square pump pulse, the available frequency span of the K spectrum can reach up to 200MHz, which is larger than fourfold of 48MHz-linewidth of Brillouin gain spectrum. For a single-slope assisted BOTDA, dynamic strain measurement with the maximum strain of 2467.4με and the vibration frequency components of 10.44Hz and 20.94Hz is obtained. For a multi-slope-assisted BOTDA, dynamic measurement with the strain variation up to 5372.9με and the vibration frequency components of 5.58Hz and 11.14Hz is achieved by using FAT to extend the strain range.

References and links

1. X. Bao and L. Chen, "Recent Progress in Brillouin Scattering Based Fiber Sensors," Sensors (Basel) **11**(12), 4152–4187 (2011).
2. L. Thévenaz, "Brillouin distributed time-domain sensing in optical fibers: state of the art and perspectives," Front. Optoelectron. China **3**(1), 13–21 (2010).
3. N. Hayashi, Y. Mizuno, and K. Nakamura, "Simplified Configuration of Brillouin Optical Correlation-Domain Reflectometry," IEEE Photonics J. **6**(5), 1–7 (2014).
4. N. Hayashi, Y. Mizuno, and K. Nakamura, "Alternative Implementation of Simplified Brillouin Optical Correlation-Domain Reflectometry," IEEE Photonics J. **6**(6), 1–8 (2014).
5. N. Hayashi, Y. Mizuno, and K. Nakamura, "Simplified Brillouin Optical Correlation-Domain Reflectometry Using Polymer Optical Fiber," IEEE Photonics J. **7**(1), 1–7 (2015).
6. K. Hotate, "Fiber distributed Brillouin sensing with optical correlation domain techniques," Opt. Fiber Technol. **19**(6 6, Part B), 700–719 (2013).
7. K. Hotate and M. Tanaka, "Distributed fiber Brillouin strain sensing with 1-cm spatial resolution by correlation-based continuous-wave technique," IEEE Photonics Technol. Lett. **14**(2), 179–181 (2002).
8. K. Y. Song, Z. He, and K. Hotate, "Distributed strain measurement with millimeter-order spatial resolution based on Brillouin optical correlation domain analysis," Opt. Lett. **31**(17), 2526–2528 (2006).
9. D. Garus, T. Gogolla, K. Krebber, and F. Schliep, "Distributed sensing technique based on Brillouin optical-fiber frequency-domain analysis," Opt. Lett. **21**(17), 1402–1404 (1996).
10. D. Garcus, T. Gogolla, K. Krebber, and F. Schliep, "Brillouin optical-fiber frequency-domain analysis for distributed temperature and strain measurements," J. Lightwave Technol. **15**(4), 654–662 (1997).
11. A. Minardo, R. Bernini, and L. Zeni, "Brillouin optical frequency domain analysis in polymer optical fiber," (2014), pp. 91576V–91576V–91574.
12. R. Bernini, A. Minardo, and L. Zeni, "Distributed Sensing at Centimeter-Scale Spatial Resolution by BOFDA: Measurements and Signal Processing," IEEE Photonics J. **4**(1), 48–56 (2012).

13. Z. Ma, M. Zhang, Y. Liu, X. Bao, H. Liu, Y. Zhang, and Y. Wang, "Incoherent Brillouin Optical Time-Domain Reflectometry With Random State Correlated Brillouin Spectrum," IEEE Photonics J. **7**(4), 1–7 (2015).
14. Y. Weng, E. Ip, Z. Pan, and T. Wang, "Single-end simultaneous temperature and strain sensing techniques based on Brillouin optical time domain reflectometry in few-mode fibers," Opt. Express **23**(7), 9024–9039 (2015).
15. Z. N. Wang, J. Li, M. Q. Fan, L. Zhang, F. Peng, H. Wu, J. J. Zeng, Y. Zhou, and Y. J. Rao, "Phase-sensitive optical time-domain reflectometry with Brillouin amplification," Opt. Lett. **39**(15), 4313–4316 (2014).
16. Y. Dong, H. Zhang, L. Chen, and X. Bao, "2 cm spatial-resolution and 2 km range Brillouin optical fiber sensor using a transient differential pulse pair," Appl. Opt. **51**(9), 1229–1235 (2012).
17. Y. Dong, L. Chen, and X. Bao, "Extending the Sensing Range of Brillouin Optical Time-Domain Analysis Combining Frequency-Division Multiplexing and In-Line EDFAs," J. Lightwave Technol. **30**(8), 1161–1167 (2012).
18. Y. Dong, P. Xu, H. Zhang, Z. Lu, L. Chen, and X. Bao, "Characterization of evolution of mode coupling in a graded-index polymer optical fiber by using Brillouin optical time-domain analysis," Opt. Express **22**(22), 26510–26516 (2014).
19. A. Minardo, R. Bernini, and L. Zeni, "Analysis of SNR penalty in Brillouin optical time-domain analysis sensors induced by laser source phase noise," J. Opt. **18**(2), 025601 (2016).
20. A. Dominguez-Lopez, X. Angulo-Vinuesa, A. Lopez-Gil, S. Martin-Lopez, and M. Gonzalez-Herraez, "Non-local effects in dual-probe-sideband Brillouin optical time domain analysis," Opt. Express **23**(8), 10341–10352 (2015).
21. J. Urricelqui, M. Sagues, and A. Loayssa, "Phasorial differential pulse-width pair technique for long-range Brillouin optical time-domain analysis sensors," Opt. Express **22**(14), 17403–17408 (2014).
22. L. Thévenaz, S. F. Mafang, and J. Lin, "Effect of pulse depletion in a Brillouin optical time-domain analysis system," Opt. Express **21**(12), 14017–14035 (2013).
23. Y. Mao, N. Guo, K. L. Yu, H. Y. Tam, and C. Lu, "1-cm-Spatial-Resolution Brillouin Optical Time-Domain Analysis Based on Bright Pulse Brillouin Gain and Complementary Code," IEEE Photonics J. **4**(6), 2243–2248 (2012).
24. A. W. Brown, B. G. Colpitts, and K. Brown, "Dark-Pulse Brillouin Optical Time-Domain Sensor With 20-mm Spatial Resolution," J. Lightwave Technol. **25**(1), 381–386 (2007).
25. P. Xu, Y. Dong, J. Zhang, D. Zhou, T. Jiang, J. Xu, H. Zhang, T. Zhu, Z. Lu, L. Chen, and X. Bao, "Bend-insensitive distributed sensing in singlemode-multimode-singlemode optical fiber structure by using Brillouin optical time-domain analysis," Opt. Express **23**(17), 22714–22722 (2015).
26. A. Minardo, A. Coscetta, L. Zeni, and R. Bernini, "High-Spatial Resolution DPP-BOTDA by Real-Time Balanced Detection," IEEE Photonics Technol. Lett. **26**(12), 1251–1254 (2014).
27. Y. Koyamada, Y. Sakairi, N. Takeuchi, and S. Adachi, "Novel Technique to Improve Spatial Resolution in Brillouin Optical Time-Domain Reflectometry," IEEE Photonics Technol. Lett. **19**(23), 1910–1912 (2007).
28. W. Li, X. Bao, Y. Li, and L. Chen, "Differential pulse-width pair BOTDA for high spatial resolution sensing," Opt. Express **16**(26), 21616–21625 (2008).
29. M. A. Soto, G. Bolognini, F. Di Pasquale, and L. Thévenaz, "Long-range Brillouin optical time-domain analysis sensor employing pulse coding techniques," Meas. Sci. Technol. **21**(9), 094024 (2010).
30. X. Angulo-Vinuesa, S. Martin-Lopez, P. Corredera, and M. Gonzalez-Herraez, "Raman-assisted Brillouin optical time-domain analysis with sub-meter resolution over 100 km," Opt. Express **20**(11), 12147–12154 (2012).
31. Z. Li, L. Yan, L. Shao, W. Pan, and B. Luo, "Coherent BOTDA sensor with intensity modulated local light and IQ demodulation," Opt. Express **23**(12), 16407–16415 (2015).
32. Y. Lu, Z. Qin, P. Lu, D. Zhou, L. Chen, and X. Bao, "Distributed Strain and Temperature Measurement by Brillouin Beat Spectrum," IEEE Photonics Technol. Lett. **25**(11), 1050–1053 (2013).
33. Y. Peled, A. Motil, and M. Tur, "Fast Brillouin optical time domain analysis for dynamic sensing," Opt. Express **20**(8), 8584–8591 (2012).
34. Y. Dong, D. Ba, T. Jiang, D. Zhou, H. Zhang, C. Zhu, Z. Lu, H. Li, L. Chen, and X. Bao, "High-Spatial-Resolution Fast BOTDA for Dynamic Strain Measurement Based on Differential Double-Pulse and Second-Order Sideband of Modulation," IEEE Photonics J. **5**(3), 2600407 (2013).
35. Y. Peled, A. Motil, L. Yaron, and M. Tur, "Slope-assisted fast distributed sensing in optical fibers with arbitrary Brillouin profile," Opt. Express **19**(21), 19845–19854 (2011).
36. R. Bernini, A. Minardo, and L. Zeni, "Dynamic strain measurement in optical fibers by stimulated Brillouin scattering," Opt. Lett. **34**(17), 2613–2615 (2009).
37. Q. Cui, S. Pamukcu, W. Xiao, and M. Pervizpour, "Truly Distributed Fiber Vibration Sensor Using Pulse Base BOTDA With Wide Dynamic Range," IEEE Photonics Technol. Lett. **23**(24), 1887–1889 (2011).
38. A. Minardo, A. Coscetta, R. Bernini, and L. Zeni, "Heterodyne slope-assisted Brillouin optical time-domain analysis for dynamic strain measurements," J. Opt. **18**(2), 025606 (2016).
39. A. Motil, O. Danon, Y. Peled, and M. Tur, "Pump-Power-Independent Double Slope-Assisted Distributed and Fast Brillouin Fiber-Optic Sensor," IEEE Photonics Technol. Lett. **26**(8), 797–800 (2014).
40. D. Ba, B. Wang, D. Zhou, M. Yin, Y. Dong, H. Li, Z. Lu, and Z. Fan, "Distributed measurement of dynamic strain based on multi-slope assisted fast BOTDA," Opt. Express **24**(9), 9781–9793 (2016).
41. R. W. Boyd, *Nonlinear Optics* (Academic) 3rd edition, Chap. 9.
42. A. Zornoza, M. Sagues, and A. Loayssa, "Self-Heterodyne Detection for SNR Improvement and Distributed Phase-Shift Measurements in BOTDA," J. Lightwave Technol. **30**(8), 1066–1072 (2012).
43. J. Urricelqui, M. Sagues, and A. Loayssa, "BOTDA measurements tolerant to non-local effects by using a phase-modulated probe wave and RF demodulation," Opt. Express **21**(14), 17186–17194 (2013).

44. X. Tu, Q. Sun, W. Chen, M. Chen, and Z. Meng, "Vector Brillouin Optical Time-Domain Analysis With Heterodyne Detection and IQ Demodulation Algorithm," IEEE Photonics J. **6**(2), 1–8 (2014).
45. J. Urricelqui, A. Zornoza, M. Sagues, and A. Loayssa, "Dynamic BOTDA measurements based on Brillouin phase-shift and RF demodulation," Opt. Express **20**(24), 26942–26949 (2012).
46. M. Pagani, D. Marpaung, and B. J. Eggleton, "Ultra-wideband microwave photonic phase shifter with configurable amplitude response," Opt. Lett. **39**(20), 5854–5857 (2014).
47. are Z. Zhu, D. J. Gauthier, Y. Okawachi, J. E. Sharping, A. L. Gaeta, R. W. Boyd, and A. E. Willner, "Numerical study of all-optical slow-light delays via stimulated Brillouin scattering in an optical fiber," J. Opt. Soc. Am. B **22**(11), 2378–2384 (2005).
48. A. Lopez-Gil, M. A. Soto, X. Angulo-Vinuesa, A. Dominguez-Lopez, S. Martin-Lopez, L. Thévenaz, and M. Gonzalez-Herraez, "Evaluation of the accuracy of BOTDA systems based on the phase spectral response," Opt. Express **24**(15), 17200–17214 (2016).
49. Z. Li, L. Yan, L. Shao, W. Pan, B. Luo, J. Liang, and H. He, "Coherent BOTDA Sensor With Single-Sideband Modulated Probe Light," IEEE Photonics J. **8**(1), 1–8 (2016).

1. Introduction

Distributed optical fiber sensor systems based on Brillouin scattering have been extensively studied and discussed for structural health monitoring in diverse fields over the past two decades [1, 2], because they have the capacity for measuring the distributed strain and temperature. Brillouin scattering is generated as a result of the refractive index variations induced by the thermal motion of molecules inside the fiber creating sound-frequency waves (i.e. acoustic phonons), which can scatter incident light with a Doppler frequency shift in the order of 10GHz for a standard single-mode fiber. Up to now, several schemes to obtain distributed strain/temperature have been implemented in the correlation-domain [3–8], the frequency-domain [9–12] and the time-domain [13–25]. Among them the Brillouin optical time-domain analysis (BOTDA) has drawn great interest due to its high spatial resolution [16, 23, 26–28] and the long sensing range [17, 21, 29, 30]. The basic approach of the classical BOTDA is based on the pump-probe regime that a high-frequency pump pulse and a counter-propagating continuous probe wave with the low-frequency are injected into the fiber. When the frequency difference between pump and probe is equal to the Brillouin frequency shift (BFS) of the fiber, the energy transfer from the high-power pump to the probe wave occurs due to the stimulated Brillouin scattering (SBS). The BFS along the fiber, which is in linear relation to the strain or temperature, can be obtained by frequency-sweeping the probe wave and then the Lorentzian or Gaussian fitting the Brillouin gain spectrum (BGS) [28, 31, 32]. Nevertheless, the dynamic measurement of BOTDA systems is restricted by the process speed of the frequency-sweeping and the curve fitting.

Recently, dynamic measurement based on BOTDA has become a hot topic. On one hand, a fast BOTDA (F-BOTDA) system is proposed to quickly reconstruct the BGS, in which 100 sweeping-frequency segments of probe wave are temporal-cascaded by a fast-switching arbitrary waveform generator (AWG) [33]. Then, an improved F-BOTDA is developed by using the differential double pulses to obtain a high spatial resolution of 20cm and the second order sideband modulation to reduce the bandwidth requirement of the AWG [34]. However, the demodulation of BFS through complex curve-fitting algorithms is also time-consuming and subsequently not suitable for real time on-line monitoring. On the other hand, a slope-assisted BOTDA (SA-BOTDA) for fast strain variations measurement is proposed by only single pump pulse and using a single-slope of the local Brillouin gain spectrum [35–38].The strain vibration frequency of this system is only determined by the fiber length and average number, but its maximum strain vibration range is limited to the narrow-slope of BGS (~30MHz for single-mode fiber). A double slope-assisted BOTDA is proposed to be immune to pump pulse power variations by using both side slopes of the BGS [39]. Whereas, the maximum dynamic strain ranges of these schemes are still less than 1000με [36]. A multi-slope assisted fast BOTDA is realized based on the double-slope demodulation and frequency-agile technique (FAT), which can extend the measurement range by adding the frequency segments number of probe wave [40].

Meanwhile, different from the Brillouin gain-based BOTDA systems as mentioned above, several novel BOTDA systems which combine the Brillouin gain and phase-shift [41, 42] are employed to improve the system performance such as increasing the signal-to-noise ratio

(SNR) [42] and tolerant of the non-local effects [43]. A vector BOTDA (VBOTDA) [44] is reported using the heterodyne detection and the IQ demodulation algorithm, which can simultaneously demodulate both of the distributed BGS and Brillouin phase-shift spectra (BPSS). Then a radio frequency (RF) phase-shift with $\arctan\left(2\Delta v/\Delta v_B\right)$ that has relation to the Brillouin gain and Brillouin phase-shift is obtained using a phase-modulated probe wave and RF demodulation, which can be used to dynamic measurements due to its immunity to the power fluctuation of pump pulse and a wide available slope [43, 45].

In this paper, we define a dimensionless coefficient K as the ratio of Brillouin phase-shift to gain in the vector SBS effect, which shows a linear proportional relationship with the frequency detuning for the continuous pump and probe waves. Then a slope-assisted BOTDA system based on vector SBS and FAT is proposed and it is not only immune to the variation of pump power but also can full use of the frequency span of vector SBS beyond 200MHz for 30ns-square pump pulse. A single-slope-assisted BOTDA is executed by using the large-available frequency span of the slope and a dynamic strain measurement with strain variation of 2467.4με and the major vibration frequency of 10.44Hz is obtained. A multi-slope-assisted BOTDA is implemented by using the FAT to extend the measurement range and a dynamic measurement with the maximum strain variation up to 5372.9με and the major vibration frequency of 5.58Hz is achieved.

2. Principle

2.1 BFS demodulation based on the coefficient K spectrum

Figure 1 shows the principle of the vector SBS process [44] for the probe wave. When the frequency difference between the pump and probe is equal to the BFS (i.e. v_B) of the fiber, the probe wave would experience both the Brillouin amplification and the Brillouin phase-shift. The equations of Brillouin gain and phase-shift for a continuous probe wave are given [44, 46–48]:

$$g_{SBS}(v_S,z)=g_0\frac{\Delta v_B^2}{4\Delta v^2+\Delta v_B^2}\otimes P_P(v_P,z) \tag{1a}$$

$$\varphi_{SBS}(v_S,z)=g_0\frac{2\Delta v_B\Delta v}{4\Delta v^2+\Delta v_B^2}\otimes P_P(v_P,z) \tag{1b}$$

where g_0 is the line center gain factor, Δv_B is the Brillouin linewidth, $\Delta v = v_P - (v_S + v_B)$ is the detuning value of the probe wave from the center of BGS, $P_P(v_P,z)$ is the power spectrum of the pump pulse wave, $\otimes$ represents the convolution operator. Equation (1) represents that the Brillouin gain and the Brillouin phase-shift are the function of the frequency detuning and the optical pump pulse's power and width.
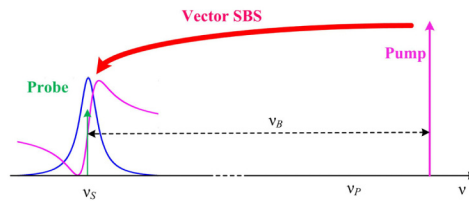

Fig. 1. Principle of the SBS process for probe wave.

Then, we define a dimensionless coefficient K as follows,

$$K(v_S,z)=\frac{\varphi_{SBS}(v_S,z)}{g_{SBS}(v_S,z)} \tag{2a}$$

Considering a rectangular-shaped pump pulse wave, its power spectrum is given by,

$$P_P(v_P, z) = P_0 \left[\frac{\sin \pi (v_p - v_0) \tau_P}{\pi (v_p - v_0)} \right]^2 \qquad (2b)$$

where v_0 is the optical carrier frequency of pump pulse, P_0 is the power of optical pump pulse, τ_P is the width of pump pulse. The coefficient K spectrum (KS) is also the function of the frequency detuning. According to the properties of the convolution, the pump power term P_0 can be eliminated in Eq. (2a), which means that KS is immune to the pump power fluctuation and its SNR will be improved.

Considering a continuous-wave (CW) pump pulse, the Eq. (2a) can be simplified as,
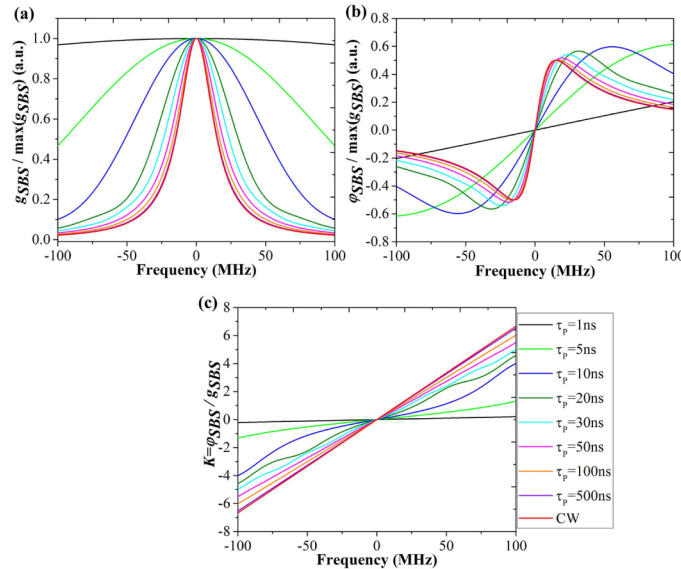
$$K(v_S, z) = \frac{2\Delta v}{\Delta v_B} \qquad (2c)$$

Fig. 2. Simulation of (a) BGS, (b) BPSS and (c) the coefficient K spectrum for different pump pulses.

By setting $\Delta v_B = 30\text{MHz}$, we simulate the BGS, BPSS and KS as shown in Fig. 2 (a), (b) and (c), respectively, with the width of pump pulse increasing from 1ns to continuous wave (CW). As the width of pump pulse decreases, both of the BGS and BPSS are broadened but the KS drops. For the width from 10ns to 30ns, the KS in the detuning frequency span from -100MHz to 100MHz is deviated away from linear curve, which can be fitted by the polynomial fitting. If the frequency span is extended, the order of the polynomial fitting should be increased to obtain a good fitting precision. As the width increase up to 50ns, the KS is close to a straight line (red line) which is the intrinsic KS with the slope of $2/\Delta v_B$ in case of the continuous pump wave. All the KSs are zero symmetry, which means that the BFS can be easily obtained by calculating the frequency at $K = 0$ through the polynomial fitting.

Thanks to the above advantages, the KS featured a wide monotonic slope range is suitable for demodulating the BFS in BOTDA resulting in large-strain range, high vibration frequency and long-distance dynamic measurement.

2.2 Heterodyne detection and IQ demodulation

The distributed BGS and BPSS of the BOTDA can be simultaneously measured by the methods proposed in [44]. For the heterodyne detection, a coherent optical reference wave (Ref-wave) as illustrated in Fig. 3 is introduced to interact with the probe wave resulting beat signal that contains the amplitude and phase information of the probe wave. Note that the frequency difference f_0 should be high enough to avoid the interaction between Ref-wave and pump pulse through SBS effect. At positon z, the optical field can be represented by,

$$E(v_S, z) = E_S \exp(g(v_S, z)) \exp(j2\pi v_S t + j\varphi_B(v_S, z)) + E_R \exp(j2\pi(v_S + f_0)t) \quad (3)$$

where E_S and E_R are the amplitude of the optical fields of probe and Ref-wave. Then, the optical beat signal generated by the interaction between probe and Ref-wave is detected by a high bandwidth photodetector (PD) with the AC output. The resultant RF signal can be described,

$$I(f_0) = 2R_D E_S E_R (1 + g(v_S, z)) \cos(2\pi f_0 t - \varphi_B(v_S, z)) \quad (4)$$

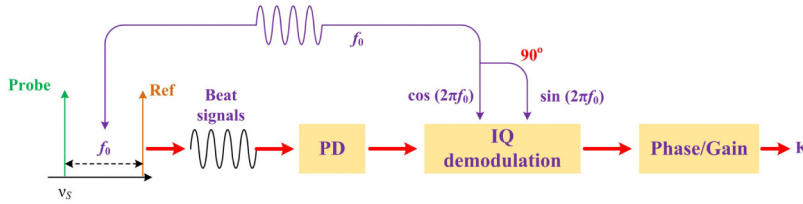where R_D is the responsive of the photo-detector.

Fig. 3. Principle of the heterodyne detection and IQ demodulation.

Then, the RF signal is demodulated by the digital signal process through IQ demodulation algorithm. After the RF signal is firstly split into two equal-power branches and separately multiplied with two orthogonal signals which has the same frequency of RF signal and then filtered out by a digital low-pass filter, two quadrature based band signals can be obtained,

$$I(v_S, z) = \frac{\sqrt{2}}{2} R_D E_S E_R E_0 (1 + g(v_S, z)) \cos(\varphi_B(v_S, z)) \quad (5a)$$

$$Q(v_S, z) = \frac{\sqrt{2}}{2} R_D E_S E_R E_0 (1 + g(v_S, z)) \sin(\varphi_B(v_S, z)) \quad (5b)$$

where E_0 is the amplitude of two orthogonal signals. Finally, the amplitude and phase of the RF signal can be calculated,

$$A(v_S, z) = \sqrt{I^2(v_S, z) + Q^2(v_S, z)}$$

$$(6a)$$

$$= \frac{\sqrt{2}}{2} R_D E_S E_R E_0 (1 + g(v_S, z))$$

$$P(v_S, z) = \arctan(\frac{Q(v_S, z)}{I(v_S, z)})$$

$$(6b)$$

$$= \varphi_B(v_S, z)$$

Equation (6b) shows the Brillouin phase-shift. The Brillouin gain can be calculated,

$$g(v_S, z) = \frac{A(v_S, z)}{A(v_S, 0)} - 1 \tag{6c}$$

where $A(v_S, 0)$ presents the amplitude of RF signal at $z = 0$ or other place that the probe wave is not amplified by SBS effect. Therefore, based on Eq. (2) and by frequency-sweeping probe wave or pump pulse, the distributed KS can be achieved.

2.3 Slope-assisted BOTDA using frequency-agile technique

Frequency-agile technique (FAT) is a method to quickly switch frequencies using a high performance arbitrary waveform generator (AWG), which has been used to generate a probe temporal frequency-modulated segments with the frequency interval of several MHz to quickly measure distributed BGS via F-BOTDA [33, 34]. The KS can be obtained by heterodyne detection and IQ demodulation and it is fitted to achieve the polynomial function regarding as the standard KS function. A single-slope-assisted BOTDA is shown in Fig. 4(a). By setting the frequency difference of pump pulse and probe wave equivalent to the BFS of the sensing fiber, when the fiber is vibrated, the distributed BFSs corresponding to $K = 0$ can be demodulated by substituting the K to the standard KS function.
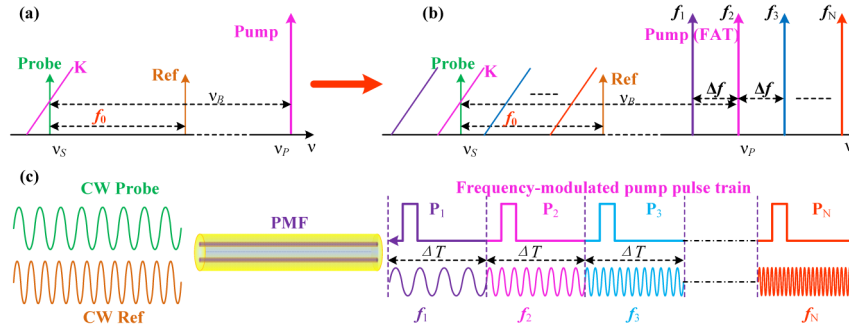

Fig. 4. Sketch map of the frequency relationship of (a) the single-slope and (b) the multi-slope assisted BOTDA based on vector SBS and FAT. (c) Multi-slope assisted BOTDA: the pump pulse train is frequency-modulated using FAT and injected into the sensing fiber with the counter-propagating probe and Ref-wave.

Although the available frequency span of KS is more than twice of the linewidth of BGS, it still cannot meet the demand for large-strain-range measurement. To increase the measurement scale, a multi-slope-assisted BOTDA based on vector SBS and FAT is proposed in Fig. 4(b). The number of the pump frequency tones is added from one tone in Fig. 4(a) up to N tones corresponding to the frequency $f_j (j = 1 : \text{N})$ with the frequency interval Δf obtaining the $K_j (j = 1 : \text{N})$ for the probe wave. Different from the method used in [40] that the probe wave is frequency-modulated using FAT, the pump wave, in our scheme as shown in the right part of Fig. 4(c), is experienced two modulation processes (needing two intensity modulators): it is firstly frequency-modulated by FAT with the frequency interval Δf and the time interval ΔT, and then intensity-modulated into optical frequency-modulated pump pulse train. After tuning the delay time of the above two modulation processes and setting the time intervals of frequency segments equivalent to that of optical pump pulses, it can be achieved that the optical pump pulse $P_j (j = 1 : \text{N})$ corresponds to the frequency of f_j. Finally, the frequency-modulated pump pulse train and the continuous probe and Ref-wave are counter-propagated into the sensing fiber. Considering the Nyquist sampling theorem, for this slope-assisted BOTDA, the maximum vibration frequency of fiber can be derived,

$$f_{\text{multi}} = \frac{1}{2} \frac{1}{N \cdot \Delta T_{\min}} \qquad (7)$$

where $\Delta T_{\min} = 2nL/c$ is equal to the roundtrip time and dependent on the fiber length, n is the refractive index of the fiber, c is the speed of light in a vacuum, L is the fiber length. It is clearly shown that the maximum vibration frequency is limited by both of the fiber length L and the frequency segments number N.

After the BGS and BPSS is measured and calculated based on heterodyne detection and IQ demodulation, the demodulation process of multi-slope assisted K-BOTDA is followed. Firstly, by setting the small frequency interval, for example Δf =4MHz , the static distributed KS will be obtained based on Eq. (2a) and it will be polynomial fitted to obtain the standard K function. Secondly, by setting the frequency interval Δf at tens or hundreds of MHz, the K_j corresponding to the frequency f_j is also calculated based on Eq. (2a) and the value $K_{\text{near}0}$, which is close to zero, can be found out. Finally, by substituting $K_{\text{near}0}$ into the standard KS function, the distributed BFS can be achieved. Note that the maximum strain range can be extended by increasing the frequency segments number N and the frequency interval Δf .

3. Experimental setup

The experimental setup depicted in Fig. 5 was assembled in order to explore the characteristic of the slope-assisted BOTDA base on vector SBS and FAT. A narrow linewidth optical fiber laser was used as the light source, which operated at the wavelength of 1550nm and output power of 80mW. Then, an optical coupler was used to split the output light into two branches. The lower-branch with 90% power component was modulated by a single sideband modulator (SSBM), which was driven by an 880MHz RF signal output from a microwave generator (MWG), generating the probe wave (carrier) and Ref-wave (+ 1th order sideband) [49] under the −1th order sideband suppression regime. Meanwhile, a Fabry–Pérot interferometer (FPI) was employed to monitor this process. An optical isolator (OI) was used to prevent the apparatus from being damaged by the high-power pump pulse. Consequently, both of continuous probe wave and Ref-wave with the total power ~2.5mW were launched into a 50-m Panda polarization-maintaining fiber (PMF) with the BFS around 10.69GHz at room temperature, where the PMF was used as the sensing fiber to eliminate the polarization fading and to reduce the average time.
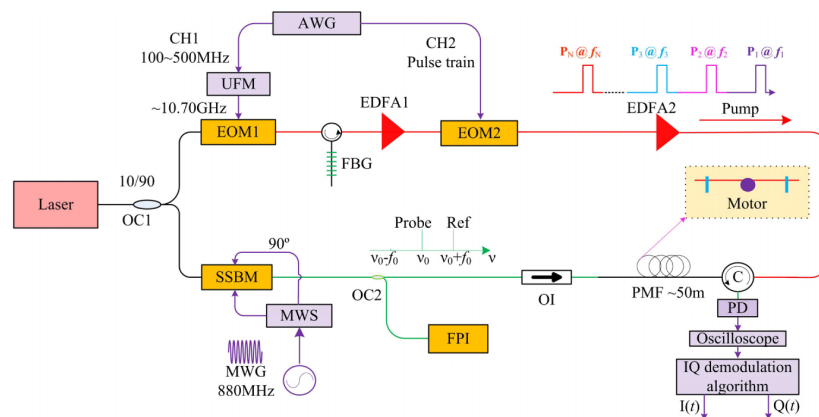

Fig. 5. Experimental setup of the slope-assisted BOTDA based on vector SBS and FAT. SSBM: single sideband modulator; MWG: microwave generator; MWS: microwave splitter; FPI: Fabry–Pérot interferometer; OI: optical isolator; C: circulator; EOM: electro-optic modulator; EDFA: erbium doped fiber amplifier; AWG, Arbitrary-waveform generator; UFM: up-converter module; FBG: fiber Bragg grating.

The upper-branch with 10% power component was firstly modulated into the optical temporal frequency-segments by the first electric-optic modulator (EOM1) which was driven by the electrical temporal frequency-segments output from the channel 1 (CH1) of AWG using the FAT under the double-sideband suppressed-carrier regime. Then the upper-sideband was extracted by a fiber Bragg grating (FBG) and amplified by an Erbium-doped fiber amplifier 1 (EDFA1). The frequency-agile span of AWG was set from 100MHz to 500MHz and an up-converter module was used to raise this span to cover the BFS of the sensing fiber. Then the optical upper-sideband wave was modulated into an optical pulse train by the second electric-optic modulator (EOM2) which was driven by the electrical pulse train output from the CH2 of AWG. The time interval of the pulses was consistent with that of the frequency segments and is set at 800ns which is longer enough to avoid the overlap of the backscattering Brillouin signals generated from two adjacent pulses. The delay time of two channels of AWG was tuned to make sure that the pulse P_j was located in the frequency segment f_j. Subsequently, the peak power of the frequency-modulated pump pulse train was amplified by EDFA2 to ~1W and the pump pulse train was counter-propagated into the PMF through an optical circulator.

Finally, the beat signal generated by the interaction between the probe wave and Ref-wave was detected by a 5-GHz bandwidth photo-detector resulting in the heterodyne RF signal which recorded the Brillouin gain and phase-shift information. Then the heterodyne RF signal was collected by the Oscilloscope (*Agilent*, MSO9254A) with the sampling rate f_{sa}=5GSa/s and demodulated by IQ demodulation algorithm to calculate the coefficient K value. An electromotor is employed to induce a periodical vibration in a section of PMF.

4. Experimental results

4.1. Measurement of K spectra for different pump pulses

In the experiment, for static strain measurement, a 3m-section of PMF is stretched without vibration and a square-type optical pulse is used as the pump pulse. The frequency segments of optical pump pulse train is scanned from $f_1 = 10.55$GHz to $f_N = 10.95$GHz with the frequency interval Δf=4MHz, corresponding to the frequency segments number $N = 101$ and the time interval ΔT=800ns. For each frequency, the data duration of the probe wave is 800ns which is larger than the roundtrip time $(\Delta T_{min}$=500ns$)$ of the PMF. Similar to the fast frequency-sweeping methods as mentioned in [33, 34] and the heterodyne detection [44], the original measured heterodyne RF signal with the duration of 50µs is tailored into the short segments with the same length $\Delta T \cdot f_{sa} = 4000$, which can be formed by a 101×4000 array. After the IQ demodulation process [44], the measured three-dimensional (3-D) BGSs and BPSSs are demodulated with the average of 128 to improve the SNR as shown in Fig. 6(a) and (b), respectively. Based on the Eq. (2), the distributed KS are calculated and shown in Fig. 6(c), (e) and (g) for the pump pulse width of 10ns, 20ns and 30ns corresponding to the spatial resolution of 1m, 2m and 3m, respectively. As a result, it is clearly seen that the strain sections are separated from the non-strain sections. However, the strain regions become narrow as the widths of pump pulse increase because the spatial resolution is decreased. The BGS (blue triangular scatter), BPSS (magenta scatter) and the KS (red square scatter) and their fitted curves at z = 13.6m are plotted in Fig. 6(d), (f) and (h) for the pump pulse width of 10ns, 20ns and 30ns, respectively. The BGS and BPSS are broadened as the pump pulse width decrease while the fluctuation of the K spectrum increase due to influence of the pump power width.

In Fig. 6(h), the BFS of 10.694GHz and the linewidth of 48.0MHz are calculated by Lorentzian-type curve fitting (blue line) the BGS. However, for the KS, a wide available frequency span (exceed 200MHz) is obtained, which is larger than fourfold of the linewidth of the BGS. The little asymmetry of three spectra maybe induced by the non-standard square-type pump pulse. Noted that the data fluctuation of the KS is better than the BGS and the

BPSS especially near the center of BGS, which shows that the KS is immune to the power fluctuation of pump pulse resulting in a better SNR. Considering the trade-off between the linearity of K spectrum and the spatial resolution, a 20-ns square pump pulse corresponding to a large available frequency span about 212MHz is selected to do the following dynamic measurements.
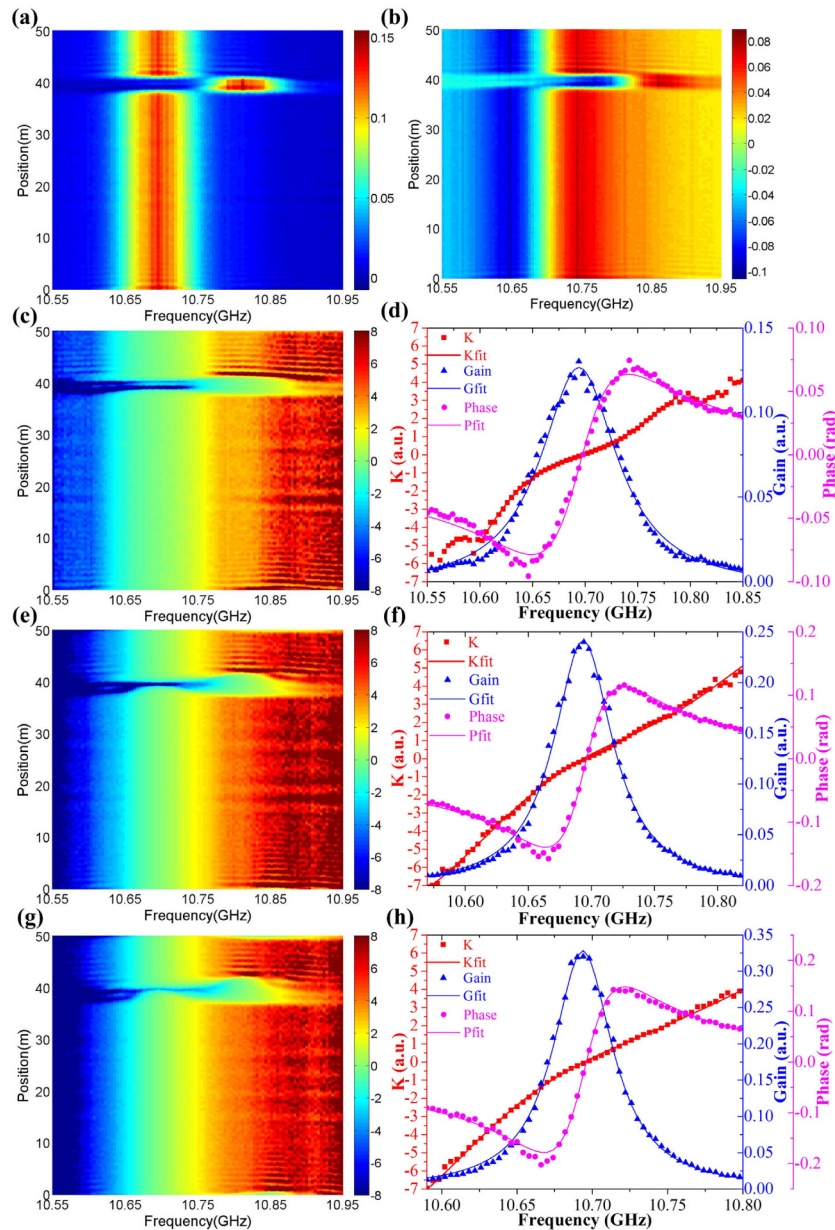

Fig. 6. The top-views of the measured 3-D (a) BGS and (b) BPSS for 10ns-pump pulse over a 50m sensing fiber. The top-views of the measured 3-D KS correspond to the pump pulse width of (c) 10ns, (e) 20ns and (g) 30ns, respectively. The BGS, BPSS and KS at z = 13.6m correspond to the pump pulse width of (d) 10ns, (f) 20ns and (h) 30ns, respectively.

The strain dependences of BFS measured by the BGS, BPSS and KS are shown in Fig. 7. The linear-fitting curves of BFS for the BGS (black line), the BPSS (blue line) and the KS

(magenta line) are achieved, which reveal good linearity with the correlation coefficients larger than 0.9990 and the strain coefficients of 0.04715MHz/µε , 0.04725MHz/µε and 0.04733MHz/µε , respectively. Furthermore, a zoom-on view is used to show the slightly difference of these three linear-fitting curves. The results mentioned above illustrate the sensing potential application of the KS.
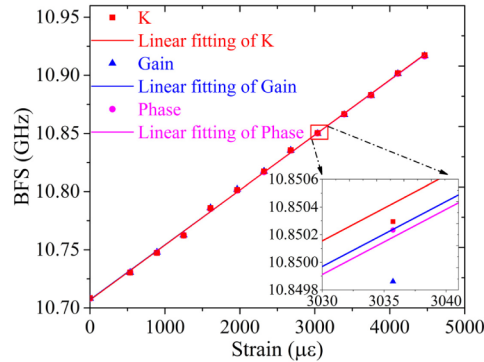

Fig. 7. The strain dependences of BFS measured by the BGS, the BPSS and the KS. Symbolic points denote the experimental data, while the solid lines are the linear fitting curves.

4.2. Single-slope-assisted BOTDA

A single-slope-assisted BOTDA system is implemented by setting f_j as a constant and the width of pump pulses to 20ns. The trace sampling rate is set at 1000 frames/s by using the segmented memory of the oscilloscope. When a 3m-section around z = 39m is vibrated by the electric-motor, the time traces of heterodyne RF signals during 512ms are quickly acquired and then they can be formed by a $512 \times (101 \times 4000)$ array. Because the data of the 101 frequency segments with the same frequency are averaged to improve the SNR, this three-dimensional array can be dimension-reduced to a 512×4000 array. Then the Brillouin gain and phase-shift and the K value over time are demodulated by IQ demodulation and Eq. (2a). The dynamic strain measurement at z = 39m as shown in Fig. 8(a) is demodulated through substituting K into the standard KS function and is fitted by the 3th polynomial function, while its power spectrum information is shown in Fig. 8(b). The maximum strain variation is about 2467.4µε (116.78MHz) and its frequency components contain a major component of 10.44Hz and a second harmonic component of 20.94Hz. It is worth nothing that the maximum vibration frequency can be reach up to 1MHz based on the Eq. (7) if the time interval ΔT is set at 500ns without average. Besides, the maximum strain variation has the potential capacity of breaking through 4000µε (189.32MHz).
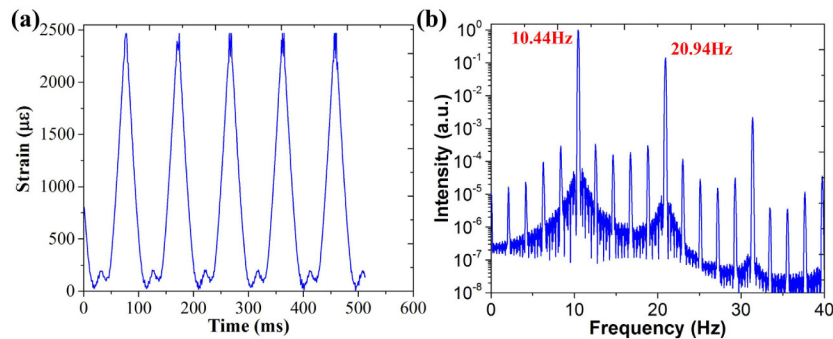

Fig. 8. (a) The dynamic strain measurements of the single-slope-assisted BOTDA and (b) its power spectrum analysis.

4.3. Multi-slope-assisted BOTDA

The time traces of the BGS, BPSS and KS in Fig. 9 are firstly measured by setting the frequency interval $\Delta f = 4\text{MHz}$. The vibration tendencies in these three figures are clearly synchronous. Then the temporal distributed BFSs calculated by the Lorentz-curve fitting for the BGS (black square) and the polynomial-fitting for the KS (blue triangle) are served as the reference time traces.
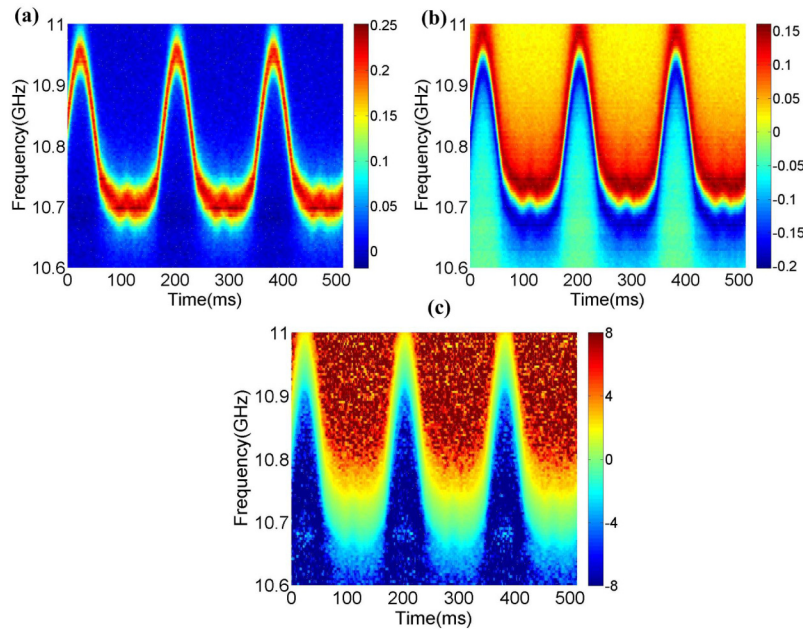

Fig. 9. The top-views of the measured 3-D (a) BGS, (b) BPSS and (c) KS over 512ms.

The dynamic strain measurements (red lines) based on multi-slope-assisted BOTDA are displayed in Fig. 10, where Fig (a), (b), (c) and (d) correspond to the frequency interval $\Delta f = 80\text{MHz}, 120\text{MHz}, 160\text{MHz}$ and 180MHz and the frequency segments number N = 6, 4, 3 and 3 respectively. A shape difference between the vibration waveform of multi-slope-assisted BOTDA and that of single-slope-assisted BOTDA is generated because the wheel of motor is enlarged to increase the strain in multi-slope-assisted BOTDA. It is clearly shown that the time traces (red line) in Fig. 10 (a), (b) and (c) measured by the multi-slope-assisted BOTDA are in good agreement with the reference time traces. However, for the time trace (red line) in Fig. 10(d) corresponding to the frequency interval $\Delta f = 180\text{MHz}$, several distortion points within blue ellipse are separated from the reference time traces, which is induced by the improperly choosing of K_{near0}, because the data fluctuation of the KS at the frequency far from BFS can be ignored at such a large frequency interval, resulting in one or more K_j which is close to 0 but the frequency is not next to BFS. Furthermore, a zoom-on view of the red boxes around the time of 290ms is shown in Fig. 10(e). Compared with the reference time traces, two time traces (green and olive lines) corresponding to the frequency intervals Δf =80MHz and 120MHz are in good agreement and the trace (magenta line) corresponding to the frequency interval Δf =160MHz has a slight distortion while a serious distortion for the trace (red line) corresponding to the frequency interval Δf =180MHz. Moreover, the correlation coefficients between the reference time traces (e.g. black square) and the demodulated time traces for the frequency interval $\Delta f = 80\text{MHz}$, 120MHz,

160MHz and 180MHz is computed as 0.9990, 0.9989, 0.9984 and 0.9870, respectively. It can be clearly seen that the correlation coefficient decreases (i.e. the measurement error increases) as the frequency interval extends. The maximum strain variation in experiment is about 5372.9µε (254.3MHz). Moreover, as shown in Fig. 10(f), the power spectrum of red-line trace, for example, corresponding to the frequency interval Δf =160MHz is almost completely coincident with that of two reference time traces (black and blue lines) and it contains a major component of 5.58Hz and a second harmonic component of 11.14Hz. It is worth nothing that the maximum vibration frequency for the frequency interval Δf =160MHz can be reached up to 0.33MHz based on the Eq. (7), if the time interval ΔT is set at 500ns equivalent to the round-trip time without average.
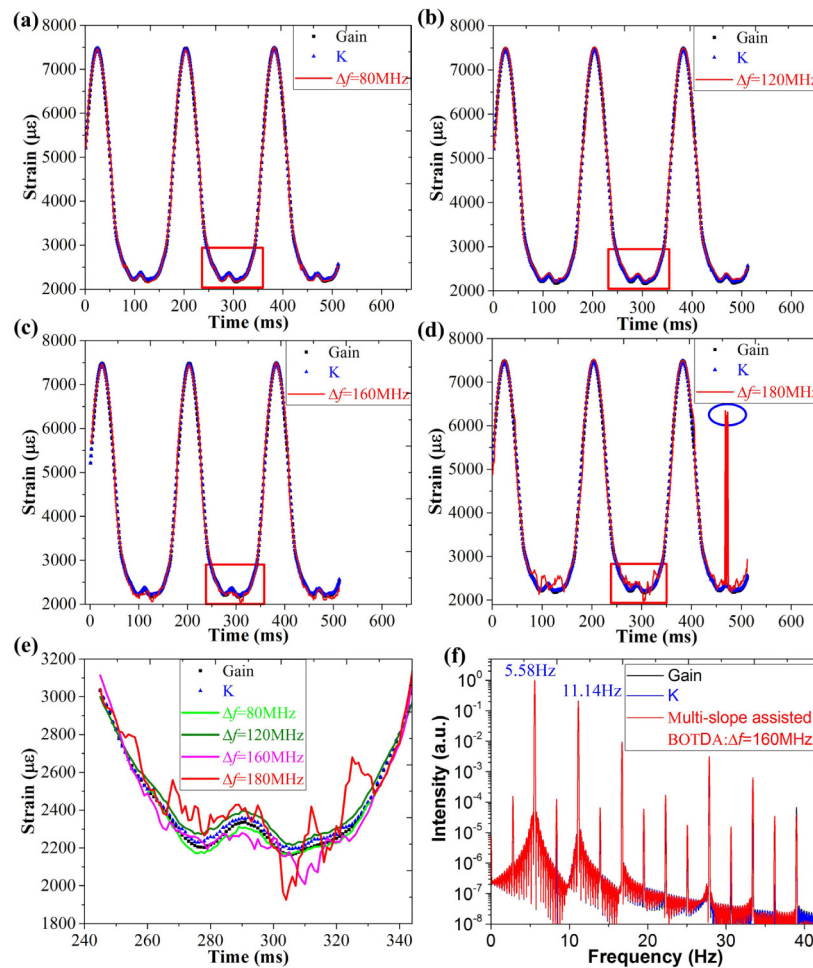

Fig. 10. The dynamic strain measurements of the multi-slope assisted BOTDA. The comparison between the reference time traces and the demodulated time traces in case of the frequency intervals (a) $\Delta f = 80\text{MHz}$, (b) $\Delta f = 120\text{MHz}$, (c) $\Delta f = 160\text{MHz}$ and (d) $\Delta f = 180\text{MHz}$. (e) A zoon on view of the time traces within the red blocks. (f) The power spectra of the reference time traces (black and blue lines) and the time trace corresponding to the frequency interval $\Delta f = 160\text{MHz}$.

5. Discussions

The KS combines the BPSS and the BGS, which not only makes full use of the frequency span of the vector SBS but also is immune to the power fluctuation of pump pulse. The BFS demodulation process is much easier than that of the traditional BOTDA [16, 28]. Differing from the RF phase-shift in [45] whose slope at the high absolute frequency detuning $|\Delta\nu|$ becomes flat and measurement range is 128MHz under a broadened spectrum for a narrow 9ns-pump pulse, the KS shows a steeper slope at the high frequency detuning $\Delta\nu$ and the available frequency span exceeding 200MHz for a 30ns-pump pulse, which implies a more precise strain demodulation at the large strain region and a long-distance sensing thanks to the wide-width pump pulse. For the single-slope-assisted-BOTDA systems, the available frequency span in this work is more than threefold of the linewidth of the BGS used in BOTDA [35]. For the multi-slope assisted systems, the maximum frequency interval Δf in this work can reach up to 160MHz while that of the gain-based BOTDA [40] is only 80MHz, which means that the frequency segment number in this work is half of that of gain-based BOTDA and the maximum strain vibration frequency in this work is twice of that of gain-based BOTDA at the same fiber length.

6. Conclusions

In this paper, we have proposed and experimentally demonstrated a slope-assisted BOTDA based on vector SBS and FAT for wide-strain-range dynamic measurements. Firstly, the KS defined as the ratio of BPSS to BGS is used in BOTDA system, which has remarkable merits: a linear function of the frequency detuning for the continuous pump and probe waves, easy to demodulate BFS, immunity to the power fluctuation of optical pump and a wide available frequency span. In experiment, an available frequency span exceeding 200MHz of the KS is measured for a 30ns-square-pump pulse, which is larger than fourfold of the 48.0MHz-linewidth of the BGS. Secondly, a maximum strain variation of 2467.4με (116.78MHz) with frequency components of 10.44Hz and 20.94Hz is measured by the single-slope-assisted BOTDA. Finally, dynamic measurements with the strain variation of 5372.9με (254.3MHz) and the vibration frequency components of 5.58Hz and 11.14Hz are achieved by the multi-slope-assisted BOTDA. The measurement range of strain variation can be easily extended by adding the frequency segment number while the maximum vibration frequency measured is determined by the sensing fiber length and the frequency segment number.